Volume 14 | Number 46 | 14 December 2016 | Pages 10735–11016

Organic & Biomolecular Chemistry

www.rsc.org/obc

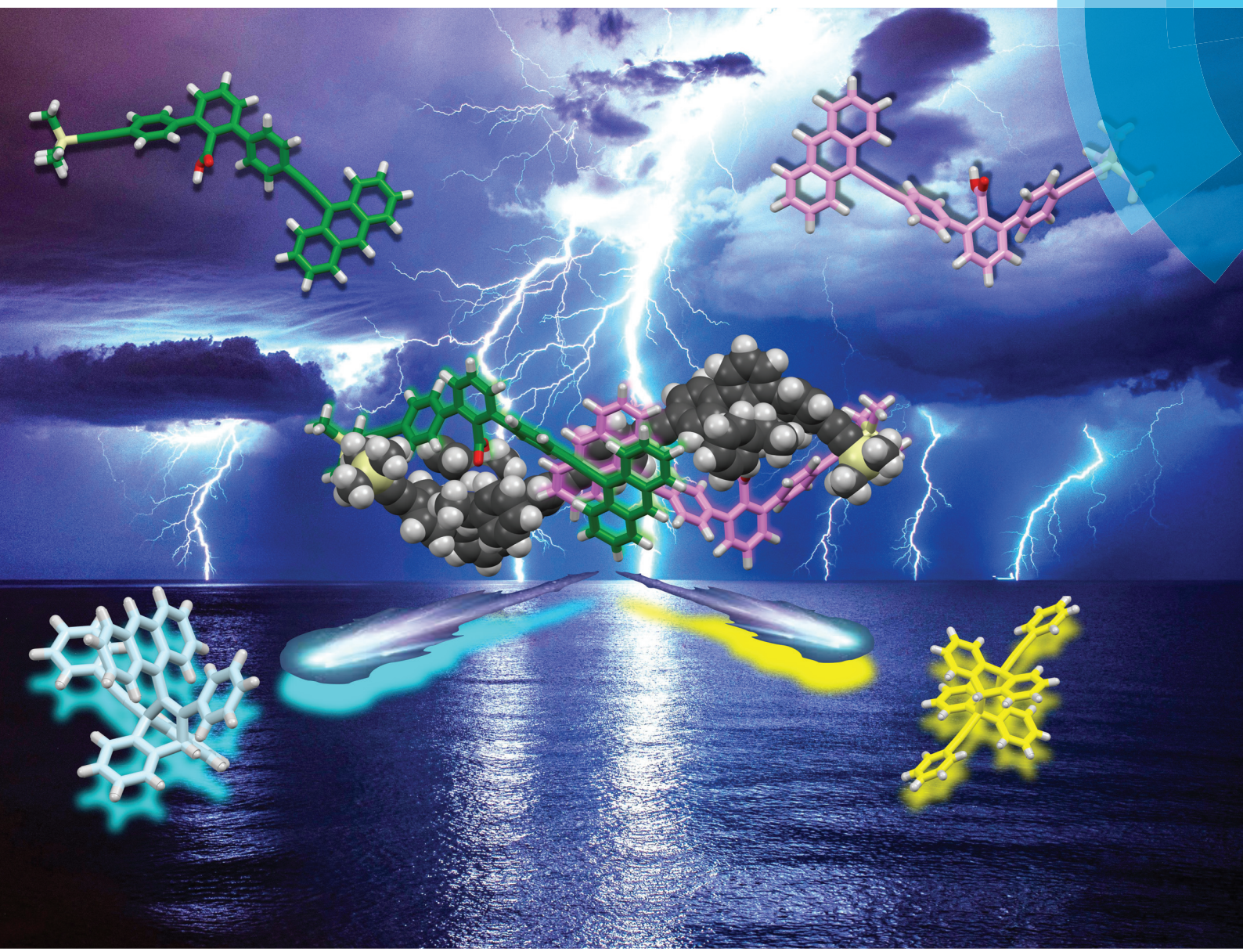

ISSN 1477-0520

ROYAL SOCIETY OF CHEMISTRY

PAPER

Eiji Yashima *et al.*

Remarkable acceleration of template-directed photodimerisation of 9-phenylethynylanthracene derivatives assisted by complementary salt bridge formation

175 YEARS

Organic & Biomolecular Chemistry

PAPER

View Article Online
View Journal | View Issue

Cite this: *Org. Biomol. Chem.*, 2016, **14**, 10822

Remarkable acceleration of template-directed photodimerisation of 9-phenylethynylanthracene derivatives assisted by complementary salt bridge formation†

Junki Tanabe, Daisuke Taura, Naoki Ousaka and Eiji Yashima*

Received 23rd September 2016,
Accepted 12th October 2016

DOI: 10.1039/c6ob02087a

www.rsc.org/obc

The photoirradiation of 9-phenylethynylanthracene in degassed chloroform and benzene afforded not only a [4 + 2]-*anti* Diels–Alder addition dimer, but also a [4 + 4]-*anti*-dimer as a minor product for the first time as revealed by single-crystal X-ray analysis, while the anthracene residue was quantitatively oxidised in undegassed dilute chloroform, giving the corresponding endoperoxides. The photochemical reactions of carboxylic acid monomers bearing a 9-phenylethynylanthracene unit at one and both ends were further investigated in the presence and absence of the complementary amidine dimer as the template. It was found that a similar photooxidation reaction of the monomers was significantly suppressed in the presence of the template even in undegassed chloroform. In addition, the template-directed photodimerisation of the mono- and di-9-phenylethynylanthracene-bound monomers was remarkably accelerated 30- or 61-fold in the degassed chloroform, giving the [4 + 2]-*anti*- and [4 + 4]-*anti*-dimers as major and minor products, respectively, whereas the di-9-phenylethynylanthracene-bound monomer was preferentially photo-polymerised in the absence of the template.

Introduction

Photochemical reactions often promote the formation of products inaccessible by thermal reactions, leading to one of the key reactions in the state-of-the-art organic synthesis.[1] However, it remains difficult to control the selectivity and specificity during the photochemical transformations in homogeneous solutions in a predictable way, thus producing a mixture of regioisomers along with stereoisomers. Therefore, the template-directed photoreaction has been developed not only to improve the efficiency, but also to control the regioselectivity and/or enantioselectivity.[2]

Among a variety of photoreactions, the photodimerisation of anthracene and its derivatives is one of the most well-known photochemical reactions and has been extensively investigated.[3] The photodimers are connected by two covalent bonds resulting from the [4 + 4] cycloaddition and revert to anthracenes thermally or under UV irradiation by using light below 300 nm. Taking advantage of this feature, the anthracene skeleton has been successfully applied to two-dimensional polymers,[4] supramolecular polymers,[5] reversible cross-linking reactions,[6] photochemical molecular switches[7] and photoinduced shape-changeable materials.[8] Another important synthetic feature during the anthracene photodimerisation is that substituted anthracenes at specific positions afford regio- and/or stereoisomers.[3] For instance, the irradiation of 9-substituted anthracenes gives two regioisomeric dimers, the [4 + 4]-*anti* and -*syn* photodimers (Fig. 1a), and the thermodynamically stable [4 + 4]-*anti* dimer is, in general, produced as a major product, whereas the energetically unfavourable [4 + 4]-*syn* dimer is regioselectively formed in specific environments, such as within micelles.[9] Supramolecular approaches using cyclic host molecules with a rigid concave cavity, such as cyclodextrins[5f,10] and cucurbit[*n*]urils,[5d,e,6e,10f,h] capable of encapsulating two anthracene molecules in close proximity, and DNA as a template,[11] have also been developed to improve the reaction yield and to control the regio- and stereo-selectivities during the photodimerisation of anthracene and its derivatives.

On the other hand, when exposed to light in the presence of oxygen, anthracene derivatives readily react with singlet oxygen to produce endoperoxides,[12] which eventually revert to the parent anthracenes and oxygen under thermolysis (Fig. 1a). However, anthracene can be effectively protected from photooxidation and dimerised in the cavity of cyclo-

Department of Molecular Design and Engineering, Graduate School of Engineering, Nagoya University, Chikusa-ku, Nagoya 464-8603, Japan.
E-mail: yashima@apchem.nagoya-u.ac.jp

† Electronic supplementary information (ESI) available: Experimental details and additional spectroscopic data. CCDC 1503774 and 1503775. For ESI and crystallographic data in CIF or other electronic format see DOI: 10.1039/c6ob02087a

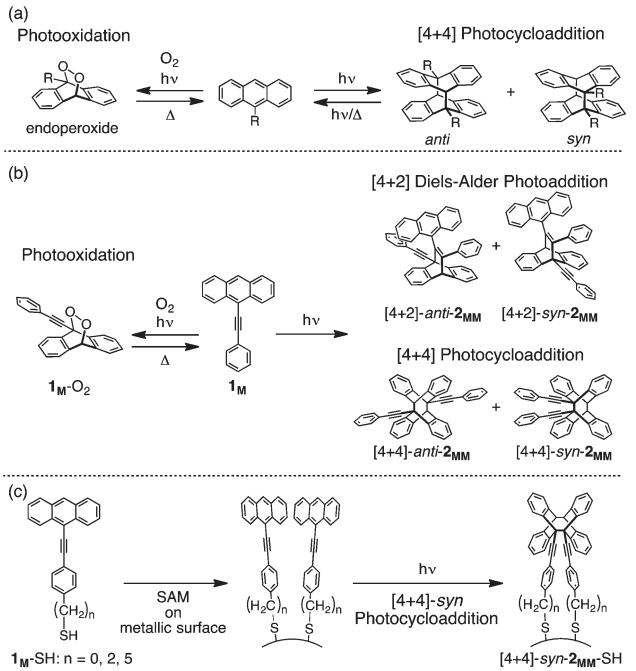

Fig. 1 Photoreaction of (a) 9-substituted anthracene, (b) 9-phenylethynylanthracene ($\mathbf{1_M}$) and (c) 9-(4-mercaptoalkylphenylethynyl)anthracenes ($\mathbf{1_M}$-SH) and their photoproducts.

dextrin[5f,10] and in the crystal state[12e] even in the presence of oxygen.

Becker and Andersson reported that the irradiation of 9-phenylethynylanthracene ($\mathbf{1_M}$) in solution readily promoted a [4 + 2] Diels–Alder addition reaction between the ethynyl moiety and the central ring of the other anthracene residue of $\mathbf{1_M}$ over the [4 + 4] cycloaddition reaction, predominantly producing a [4 + 2]-*anti* dimer ([4 + 2]-*anti*-$\mathbf{2_{MM}}$, Fig. 1b).[13] In contrast, Weiss and co-workers demonstrated the energetically unfavourable [4 + 4]-*syn* dimer formation of thiolated 9-phenylethynylanthracenes ($\mathbf{1_M}$-SH) (Fig. 1c) upon irradiation that proceeded in a highly regioselective manner when $\mathbf{1_M}$-SH was mixed in self-assembled alkane thiolate monolayers on flat Au surfaces on which the anthracene moieties were favourably arranged in such a way that the intermolecular [4 + 4]-*syn* cycloaddition ([4 + 4]-*syn*-$\mathbf{2_{MM}}$) could be possible.[14] The regioselective [4 + 4]-*syn* dimer formation was monitored by scanning tunneling microscopy (STM)[14a] and surface-enhanced Raman spectroscopy (SERS),[14b] thus showing a significant decrease in conductivity and disappearance of the peaks due to the anthracene moiety, respectively. Recently, Klajn and co-workers also demonstrated that $\mathbf{1_M}$-SH immobilised on metallic (Au and Pd) nanoparticles dimerised in a regioselective way to yield a [4 + 4]-*syn* cycloaddition product under photoirradiation (Fig. 1c), based on the time-dependent absorption spectral changes.[15]

We previously reported a series of *m*-terphenyl-based complementary double helices that could be rationally designed and synthesised based on a modular strategy we developed using amidinium–carboxylate salt bridges through which the double helices are stabilised by double hydrogen bonds with a well-defined directionality even in polar solvents.[16] Therefore, various types of functional linkers, such as Pt(II)-acetylide[16b,e,j,l,n] and azobenzene linkages,[16d,i,m] can be introduced between the *m*-terphenyl units while maintaining the double-helical structures.[16] The complementary double-helical framework stabilised by salt bridges has recently been applied to the template-directed synthesis of complementary double helices through imine-bond forming reactions between a carboxylic acid and amidine monomers bearing either a formyl or an amino group at one end.[16i,m] The complementary dimeric templates linked by an azobenzene residue significantly accelerated the imine-bond forming reactions. However, the reactions along the complementary dimer strands as a template were limited to imine-bond forming reactions.

In this work, we synthesised new carboxylic acid monomers ($\mathbf{1_C}$ and $\mathbf{3_C}$) bearing an anthracene group at one and both ends (Fig. 2a), respectively, and investigated their template-directed photodimerisation reactions in solution in the absence and presence of the complementary amidine dimer ($\mathbf{T_{AA}}$) connected by a *p*-diethynylbenzene unit as the template (Fig. 2d). The monomers $\mathbf{1_C}$ and $\mathbf{3_C}$ possess one or two 9-phenylethynylanthracene moieties identical to $\mathbf{1_M}$, hence we anticipated the regioselective photodimerisation or polymerisation of $\mathbf{1_C}$ or $\mathbf{3_C}$, respectively, giving products with a specific regioselectivity among the following four possible regioisomers ([4 + 2]-*anti*-, [4 + 2]-*syn*-, [4 + 4]-*anti*- and [4 + 4]-*syn*-isomers, Fig. 2b and c) along with acceleration of the photoreactions in the presence of the rigid template $\mathbf{T_{AA}}$ through the salt bridges, which permit the 9-phenylethynylanthracene moieties to be arranged in close proximity (Fig. 2d).

For comparison, the photochemical dimerisation of $\mathbf{1_M}$ (Fig. 1b),[13] a model compound of $\mathbf{1_C}$ and $\mathbf{3_C}$, was also thoroughly investigated under various conditions. We found that a [4 + 4]-*anti*-dimer ([4 + 4]-*anti*-$\mathbf{2_{MM}}$) was also produced as a minor product along with the major Diels–Alder addition product, [4 + 2]-*anti*-$\mathbf{2_{MM}}$, (Fig. 1b) and then their structures were unambiguously determined by single-crystal X-ray analysis.

Results and discussion

Synthesis

9-Phenylethynylanthracene ($\mathbf{1_M}$) was prepared according to the reported method.[17] The achiral carboxylic acid monomers ($\mathbf{1_C}$ and $\mathbf{3_C}$) bearing an anthracene group at one and both ends were newly synthesised according to Schemes S3 and S5,† respectively, (see the ESI†). The *p*-phenylene-linked optically active amidine dimer ($\mathbf{T_{AA}}$)[16g] and its monomeric amidine ($\mathbf{A}$)[16a] were also prepared according to the reported methods.

Photoreactions of model monomer ($\mathbf{1_M}$)

The photoreaction of $\mathbf{1_M}$ (0.50 mM) was first investigated in undegassed $CDCl_3$ at 25 °C (run 1 in Table 1) upon light

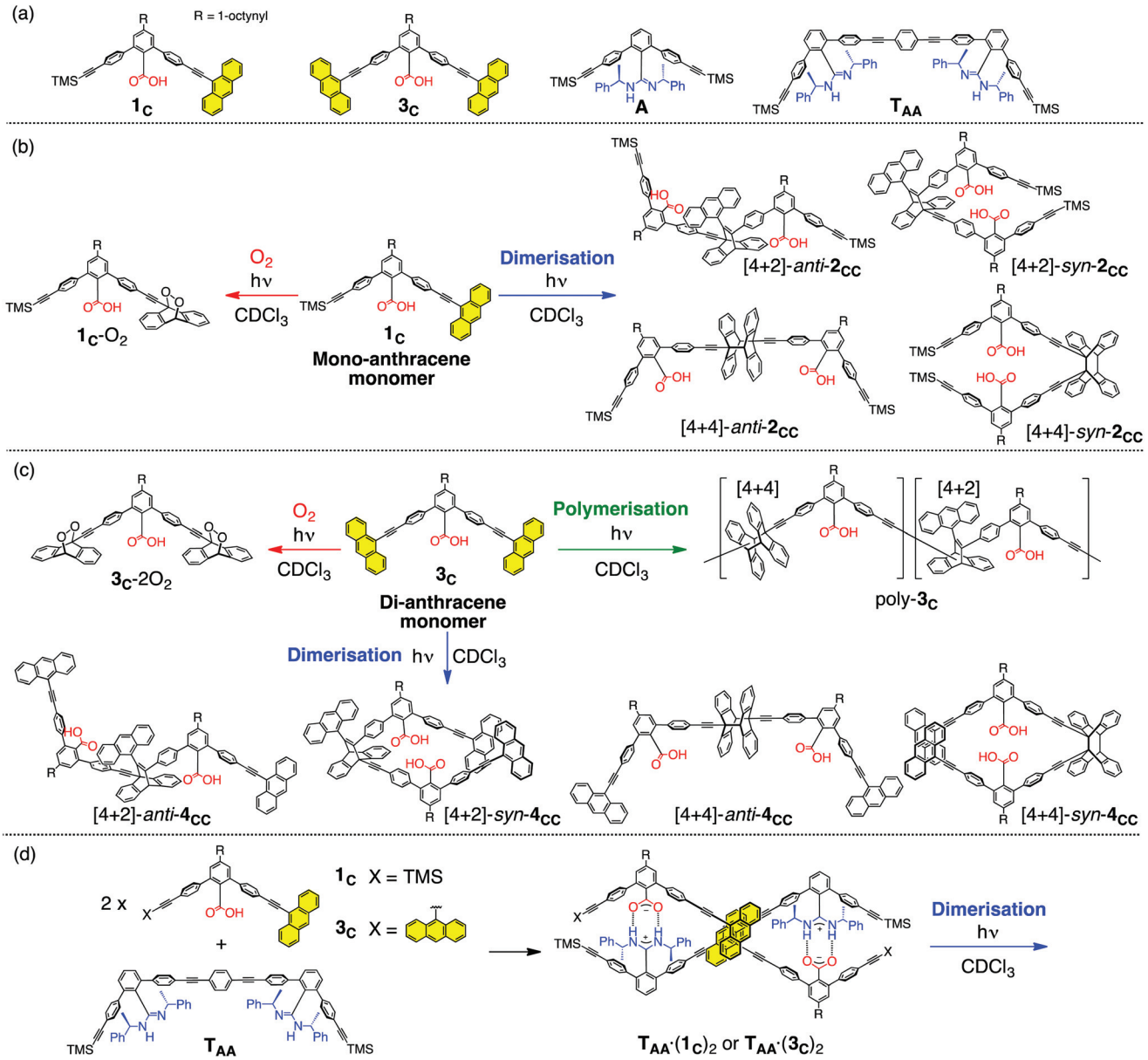

Fig. 2 (a) Chemical structures of 9-phenylethynylanthracene-bound carboxylic acid monomers ($\mathbf{1_C}$ and $\mathbf{3_C}$), monomeric amidine (**A**) and dimeric amidine template ($\mathbf{T_{AA}}$). (b and c) Possible photoreactions (photooxidation and cycloaddition reactions) of the carboxylic acid monomers ((b) $\mathbf{1_C}$ and (c) $\mathbf{3_C}$) and their photoproducts. (d) Schematic illustration for the template-directed photodimerisation of the 9-phenylethynylanthracene-bound monomers ($\mathbf{1_C}$ and $\mathbf{3_C}$).

irradiation over 400 nm. Reaction progress was monitored by ^{1}H NMR spectroscopy. The peak intensity of the anthracene proton (H_a) at the 10-position in $\mathbf{1_M}$ decreased with time, whereas a new singlet signal appeared in a relatively low magnetic field of 6.08 ppm, which can be assigned to the bridge-head proton (H_b) of endoperoxide ($\mathbf{1_M}$-O_2) and its peak intensity gradually increased as the reaction progressed, reaching 89% after irradiation for 3 min (Fig. 3a and S6a†). This assignment was supported by a molecular ionic peak at m/z = 309.19 ($[\mathbf{1_M}\text{-}O_2\text{–}H]^-$) in its negative-mode electron-spray ionisation (ESI) mass spectrum of the reaction mixture and also by the absorption spectrum of $\mathbf{1_M}$ after irradiation for 3 min, in which the peaks due to the anthracene moiety almost disappeared (Fig. S6†). It was noted that the obtained $\mathbf{1_M}$-O_2 was not stable in solution and was thermally converted back to $\mathbf{1_M}$ without decomposition at 25 °C.[12b,d,f] Thus, the rate constant for the retro-photooxidation reaction was estimated to be 4.7 × 10^{-6} s^{-1} on the basis of the time-dependent ^{1}H NMR spectral changes (Fig. S7†).

In contrast, after light irradiation of $\mathbf{1_M}$ (0.50 mM) for 30 min in degassed $CDCl_3$ at 25 °C (run 5 in Table 1), the ^{1}H NMR spectrum showed two new sets of singlet peaks due to the bridge-head protons (H'_b and H''_b) along with a new anthracene proton (H_a'), indicating the formation of two

Table 1 Results of photoreactions of $\mathbf{1_M}$ under various reaction conditions

	$\mathbf{1_M}$			Product yield (%) (Reaction rate 10^{-3} k (s^{-1}))				
Run	Solvent (conc. (mM))	Irradiation time (min)	Conv. (%) (consumption rate 10^{-3} k (s^{-1}))	$\mathbf{1_M}$-O_2	[4 + 2]-*anti*-$\mathbf{2_{MM}}$	[4 + 4]-*anti*-$\mathbf{2_{MM}}$	[4 + 2]/[4 + 4]	Sup. Fig. no.
1	Undegassed $CDCl_3$ (0.50)	3	89 (16)	89 (16)	—	—	—	Fig. S6
2	Undegassed $CDCl_3$ (8.0)	30	88 (2.0)	12[a] (0.71)	60 (0.93)	14 (0.14)	4.3	Fig. S8
3	Undegassed benzene-d_6 (0.50)	16	88 (3.2)	32[b] (1.0)	42 (0.96)	8 (0.14)	5.3	Fig. S9
4	Undegassed benzene-d_6 (8.0)	30	96 (1.9)	9[c] (0.37)	70 (1.0)	12 (0.13)	5.8	Fig. S10
5	Degassed $CDCl_3$ (0.50)	30	88 (1.7)	—	64 (1.1)	23 (0.21)	2.8	Fig. S11
6	Degassed $CDCl_3$ (8.0)	45	95 (1.5)	—	77 (1.0)	18 (0.15)	4.3	Fig. S12
7	Degassed benzene-d_6 (0.50)	30	90 (1.6)	—	74 (1.1)	15 (0.16)	4.9	Fig. S13
8	Degassed benzene-d_6 (8.0)	45	97 (1.3)	—	80 (1.0)	15 (0.13)	5.3	Fig. S14
9	Degassed benzene (8.0)	90	—[d]	—[d]	75	8	9.4	Ref. 13

[a] The maximum yield of $\mathbf{1_M}$-O_2 was 18% after 8 min irradiation of light (>400 nm) (see Fig. S8a). [b] The maximum yield of $\mathbf{1_M}$-O_2 was 38% after 8 min irradiation of light (>400 nm) (see Fig. S9a). [c] The maximum yield of $\mathbf{1_M}$-O_2 was 15% after 8 min irradiation of light (>400 nm) (see Fig. S10a). [d] Not available in ref. 13.

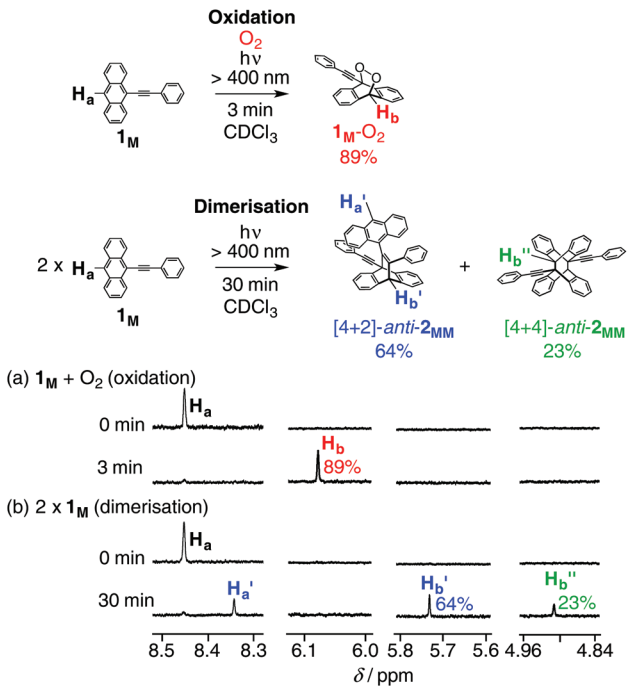

Fig. 3 Partial ^{1}H NMR (500 MHz, 25 °C) spectra of $\mathbf{1_M}$ (0.50 mM) in (a) (run 1 in Table 1) undegassed and (b) (run 5 in Table 1) degassed $CDCl_3$ before (top) and after (bottom) irradiation of light (>400 nm). Full-scale spectra are shown in Fig. S6a and S11a,† respectively.

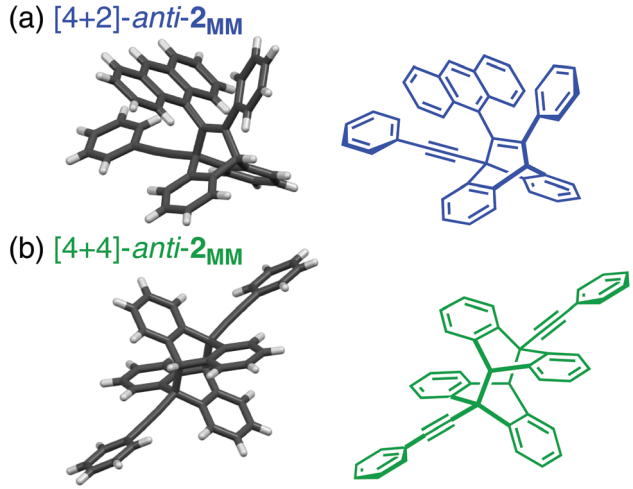

Fig. 4 The crystal structures of (a) [4 + 2]-*anti*-$\mathbf{2_{MM}}$ (CCDC 1503775) and (b) [4 + 4]-*anti*-$\mathbf{2_{MM}}$ (CCDC 1503774).

photodimers (Fig. 3b and S11a†), which were unambiguously identified as [4 + 2]-*anti*-$\mathbf{2_{MM}}$ and [4 + 4]-*anti*-$\mathbf{2_{MM}}$, respectively, by X-ray crystallographic analyses (Fig. 4) together with 2D NMR spectroscopy (Fig. S41 and S44†). Becker and Andersson reported that the photoreaction of $\mathbf{1_M}$ (8.0 mM) in degassed benzene gave [4 + 2]-*anti*-$\mathbf{2_{MM}}$ in *ca.* 75% yield together with a by-product (*ca.* 8%) which was assumed to be an intermolecular [4 + 4] cycloadduct in spite of no structural information (run 9 in Table 1).[13] Thus, we examined the photoreaction of $\mathbf{1_M}$ (8.0 mM) under almost the same conditions in degassed benzene-d_6, affording [4 + 2]-*anti*-$\mathbf{2_{MM}}$ (80%) and [4 + 4]-*anti*-$\mathbf{2_{MM}}$ (15%) after 45 min irradiation (run 8 in Table 1 and Fig. S14†). The regioisomer ratio (5.3) was different from that reported by Becker and Andersson (9.4), but the difference may not be important.

The effects of oxygen, solvent ($CDCl_3$ and benzene-d_6) and concentration (0.50 and 8.0 mM) on the photooxidation and regioselectivity ([4 + 2]/[4 + 4]) during the photoreaction of $\mathbf{1_M}$ were further investigated at 25 °C and the results are summarised in Table 1. In dilute undegassed solution, the photooxidation of $\mathbf{1_M}$ preferentially took place more than that in the concentrated solution. In particular, irradiation of a dilute solution of $\mathbf{1_M}$ (0.50 mM) in undegassed $CDCl_3$ (run 1 in Table 1) quantitatively produced $\mathbf{1_M}$-O_2 due to the heavy-atom effect of the solvent, which inhibits the photodimerisation by promoting intersystem crossing.[12c] Although the concentration and solvent effects of the photodimerisation on regioselectivity were not significant, the yield of the major product, [4 + 2]-

anti-$\mathbf{2_{MM}}$, tended to increase with the increasing concentration of $\mathbf{1_M}$ from 0.50 to 8.0 mM on changing the solvent from $CDCl_3$ to benzene-d_6.

We then calculated the structures of four possible photodimers (Fig. 1b) using the density functional theory (DFT) and found that their stabilities decrease in the following order: [4 + 2]-*anti*-$\mathbf{2_{MM}}$ > [4 + 2]-*syn*-$\mathbf{2_{MM}}$ > [4 + 4]-*anti*-$\mathbf{2_{MM}}$ > [4 + 4]-*syn*-$\mathbf{2_{MM}}$ (Fig. S5†), thus supporting the experimental results that the major product, [4 + 2]-*anti*-$\mathbf{2_{MM}}$, is much more stable than the minor one, [4 + 4]-*anti*-$\mathbf{2_{MM}}$, by 170.6 kJ mol^{-1}, whereas the corresponding *syn*-photodimers ([4 + 2]-*syn*-$\mathbf{2_{MM}}$ and [4 + 4]-*syn*-$\mathbf{2_{MM}}$) could not be observed at all in the ^{1}H NMR spectra under the present conditions even though the *syn*-Diels–Alder adduct, [4 + 2]-*syn*-$\mathbf{2_{MM}}$, is the second most stable photodimer. The reason is not clear, but it was suggested that it was due to the more favourable centrosymmetric-oriented complex formation ($(\mathbf{1_M})_2$), which could generate [4 + 2]-*syn*-$\mathbf{2_{MM}}$,[13] or these may be thermally unstable and immediately revert to the parent $\mathbf{1_M}$ in solution.

On the other hand, an energetically unfavourable [4 + 4]-*syn*-$\mathbf{2_{MM}}$ derivative was reported to form in a highly regioselective fashion on self-assembled flat metal surfaces upon photoirradiation (Fig. 1c) as revealed by STM,[14a] Raman[14b] and the time-dependent absorption spectral changes.[15]

Fig. S15† shows the experimental (top) and DFT simulated (bottom) Raman spectra of $\mathbf{1_M}$, $\mathbf{1_M}$-O_2, [4 + 2]-*anti*-$\mathbf{2_{MM}}$ and [4 + 4]-*anti*-$\mathbf{2_{MM}}$, which are in good agreement, although $\mathbf{1_M}$-O_2 contains $\mathbf{1_M}$ generated from $\mathbf{1_M}$-O_2 *via* thermolysis (Fig. S15b†).

The peaks due to the anthracene residue of $\mathbf{1_M}$ completely disappeared in the Raman spectrum of [4 + 4]-*anti*-$\mathbf{2_{MM}}$ (Fig. S15d†), while these remained in the Raman spectrum of [4 + 2]-*anti*-$\mathbf{2_{MM}}$ (Fig. S15c†). Similar distinct spectral changes were also observed in the absorption spectra of $\mathbf{1_M}$, [4 + 2]-*anti*-$\mathbf{2_{MM}}$ and [4 + 4]-*anti*-$\mathbf{2_{MM}}$ (Fig. S2a†). We note, however, that the Raman spectra of $\mathbf{1_M}$-O_2 and [4 + 4]-*anti*-$\mathbf{2_{MM}}$, in which an anthracene moiety no longer exists, were quite similar to each other except for a weak peak at 921 cm^{-1} observed for $\mathbf{1_M}$-O_2, which can be assigned to the –O–O– bond vibration (Fig. S15b†).[18] These results combined with the absorption spectra of $\mathbf{1_M}$-O_2 and [4 + 4]-*anti*-$\mathbf{2_{MM}}$ (Fig. S2a†) suggested that it might be difficult to assign the photochemical reaction products of $\mathbf{1_M}$ and its derivatives, $\mathbf{1_M}$-O_2 or [4 + 4]-*anti*-$\mathbf{2_{MM}}$, based on the Raman[14b] and absorption spectroscopies.[15] However, it is apparent that the photooxidation is protected in the absence of oxygen.

Template effects on the photoreactions of mono-9-phenylethynylanthracene-bound carboxylic acid monomer

The mono-9-phenylethynylanthracene-bound carboxylic acid monomer ($\mathbf{1_C}$) used in this study contains a 9-phenylethynylanthracene moiety identical to $\mathbf{1_M}$, probably showing a similar photoreactivity to $\mathbf{1_M}$ in the absence of the template. Based on the photoreaction results of the model monomer $\mathbf{1_M}$ (Table 1), we employed a dilute $CDCl_3$ (0.50 mM) solution throughout the following photoreactions. As anticipated, the irradiation of $\mathbf{1_C}$ in undegassed $CDCl_3$ at 25 °C (run 1 in Table 2) resulted in the formation of endoperoxide ($\mathbf{1_C}$-O_2)[19] in 89% yield after 3 min as evidenced by the bridge-head proton (H_b) that newly appeared as a singlet at 6.08 ppm (Fig. 5a and S16a†); the chemical shift was very similar to that of $\mathbf{1_M}$-O_2 (Fig. 3a and S6a†). The structure of $\mathbf{1_C}$-O_2 was characterised and identified by comparing the ^{1}H NMR spectrum of $\mathbf{1_C}$-O_2 with that of $\mathbf{1_M}$-O_2 (Fig. S1†) and ESI-mass measurements (Fig. S16c†).

The photoreactions of $\mathbf{1_C}$ (0.50 mM) in the presence of the template $\mathbf{T_{AA}}$ (0.25 mM) and its monomeric amidine **A** (0.50 mM)[20] were then investigated in undegassed $CDCl_3$ at 25 °C. The monomeric amidine **A** was used for the control experiment to evaluate the template effect of $\mathbf{T_{AA}}$ on the photoreaction. The ^{1}H NMR spectra of $\mathbf{1_C}$ (0.50 mM) in the presence of **A** (0.50 mM) or $\mathbf{T_{AA}}$ (0.25 mM) showed the characteristic peaks for the NH protons in the low magnetic field at *ca.* 13.3 ppm, indicating the salt bridge formation (Fig. S18a and S19a†).

The irradiation of $\mathbf{A{\cdot}1_C}$ (run 2 in Table 2) also produced only one set of ^{1}H NMR signals, such as H_b (6.09 ppm), resulting from the preferential formation of $\mathbf{1_C}$-O_2 complexed with **A**

Table 2 Results of photoreactions of $\mathbf{1_C}$

	$\mathbf{1_C}$				Product yield (%) (reaction rate 10^{-3} k (s^{-1}))				
Run	Additive (conc. (mM))	Solvent (conc. (mM))	Irradiation time (min)	Conv. (%) (consumption rate 10^{-3} k (s^{-1}))	$\mathbf{1_C}$-O_2	[4 + 2]-*anti*-$\mathbf{2_{CC}}$	[4 + 4]-*anti*-$\mathbf{2_{CC}}$	[4 + 2]/[4 + 4]	Sup. Fig. no.
1	—	Undegassed $CDCl_3$ (0.50)	3	89 (11)	89 (11)	—	—	—	Fig. S16
2	**A** (0.50)	Undegassed $CDCl_3$ (0.50)	3	89 (10)	89 (10)	—	—	—	Fig. S18
3	$\mathbf{T_{AA}}$ (0.25)	Undegassed $CDCl_3$ (0.50)	2	92 (25)	10[a] (4.4)	63 (11)	18 (2.5)	3.5	Fig. S19–20
4	—	Degassed $CDCl_3$ (0.50)	60	85 (0.66)	—	60 (0.40)	25 (0.11)	2.4	Fig. S21
5	**A** (0.50)	Degassed $CDCl_3$ (0.50)	90	68 (0.18)	—	19 (—)[b]	17 (0.036)	1.1	Fig. S22–24
6	$\mathbf{T_{AA}}$ (0.25)	Degassed $CDCl_3$ (0.50)	2	89 (20)	—	68 (12)	20 (2.9)	3.4	Fig. S25–26

[a] $\mathbf{1_C}$-O_2 formed during the initial stage was gradually converted into an unknown compound probably due to photolysis products of $\mathbf{1_C}$-O_2 upon further photoirradiation. The reaction rate was therefore estimated based on the time–conversion relationship during the initial stage. The maximum yield of $\mathbf{1_C}$-O_2 was 10% after 30 s irradiation of light (>400 nm) (see Fig. S19a). [b] The peaks for $(\mathbf{A})_2{\cdot}$[4 + 2]-*anti*-$\mathbf{2_{CC}}$ were too broad to estimate its reaction rate (see Fig. S22a).

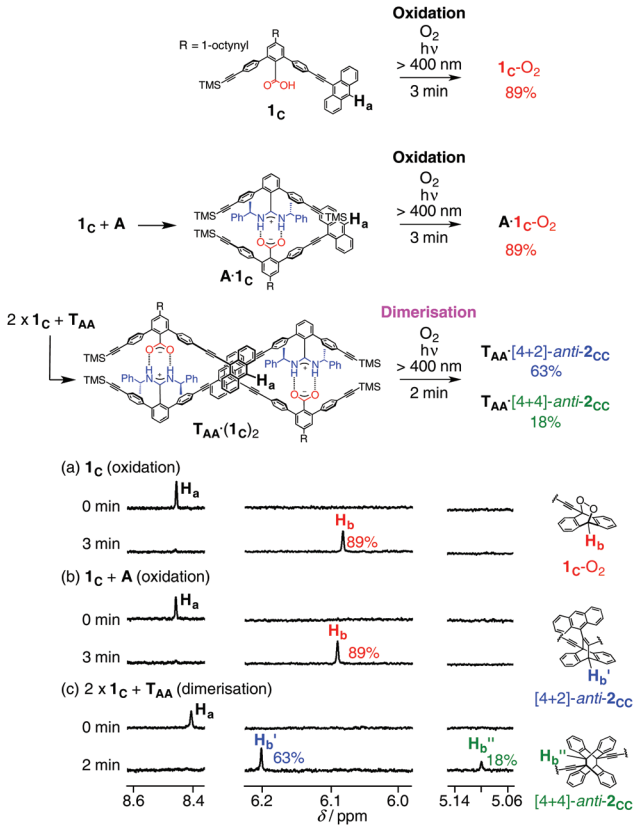

Fig. 5 Partial ^{1}H NMR (500 MHz, undegassed $CDCl_3$, 25 °C) spectra of $\mathbf{1_C}$ (0.50 mM) in the absence (run 1 in Table 2) (a) and presence of **A** (0.50 mM) (run 2 in Table 2) (b) and $\mathbf{T_{AA}}$ (0.25 mM) (run 3 in Table 2) (c) before (top) and after (bottom) irradiation of light (>400 nm). Full-scale spectra are shown in Fig. S16a, S18a and S19a.†

(Fig. 5b and S18a†) as observed in the photooxidation of $\mathbf{1_C}$ in the absence of **A** (run 1 in Table 2). In sharp contrast, upon the irradiation of $\mathbf{T_{AA}}$·$(\mathbf{1_C})_2$ (run 3 in Table 2), the peak intensity of H_a decreased and almost disappeared within 2 min, whereas two new sets of singlet peaks due to the bridge-head protons (H'_b and H''_b) appeared at 6.21 and 5.10 ppm, respectively (Fig. 5c and S19a†). These peaks could be clearly identified as the complexes of $\mathbf{T_{AA}}$·[4 + 2]-*anti*-$\mathbf{2_{CC}}$ (63%) and $\mathbf{T_{AA}}$·[4 + 4]-*anti*-$\mathbf{2_{CC}}$ (18%) based on the ^{1}H NMR spectra of the 1 : 1 mixtures of the isolated [4 + 2]-*anti*-$\mathbf{2_{CC}}$ and [4 + 4]-*anti*-$\mathbf{2_{CC}}$ after purification with $\mathbf{T_{AA}}$, respectively (Fig. S28†). Interestingly, the photooxidation reaction of $\mathbf{1_C}$ was significantly protected in the presence of the template $\mathbf{T_{AA}}$, affording $\mathbf{1_C}$-O_2 in less than 10% yield (Fig. S19a†) and the intermolecular photodimerisation selectively proceeded due to the close proximity of the two anthracene moieties arranged along the template, as supported by the decrease and red-shift of the absorption peaks of $\mathbf{1_C}$ upon the addition of $\mathbf{T_{AA}}$, indicative of the π-stacked arrangements of the anthracene moieties (Fig. S20†).

In the same way, the photoreactions of $\mathbf{1_C}$ (0.50 mM) in the absence and presence of **A** (0.50 mM) or $\mathbf{T_{AA}}$ (0.25 mM) were performed in degassed $CDCl_3$ at 25 °C (runs 4–6 in Table 2), in which the photooxidation was completely prohibited as observed in the model reaction of $\mathbf{1_M}$ under the same conditions. In the absence of **A** and $\mathbf{T_{AA}}$, $\mathbf{1_C}$ was gradually converted to the photodimers, producing [4 + 2]-*anti*-$\mathbf{2_{CC}}$ and [4 + 4]-*anti*-$\mathbf{2_{CC}}$ in 60 and 25% yields, respectively, after irradiation for 60 min (run 4 in Table 2 and Fig. 6a and S21a†).

Quite interestingly, the photodimerisation of $\mathbf{1_C}$ in the presence of the template $\mathbf{T_{AA}}$ (run 6 in Table 2) took place much faster than that in the absence of $\mathbf{T_{AA}}$, affording the $\mathbf{T_{AA}}$·[4 + 2]-*anti*-$\mathbf{2_{CC}}$ (68%) and $\mathbf{T_{AA}}$·[4 + 4]-*anti*-$\mathbf{2_{CC}}$ (20%) complexes after 2 min of light irradiation (Fig. 6c and S25a†).[21] Contrary to our expectation, however, we could not observe a specific regioselectivity during the photodimerisation, producing photodimers with an almost similar regioselectivity ([4 + 2]/[4 + 4]) to that in the absence of the template $\mathbf{T_{AA}}$.

To estimate the reaction rate constant (k) of $\mathbf{1_C}$, the conversions of $\mathbf{1_C}$ were estimated from the integral ratios of the peaks for H_a ($\mathbf{T_{AA}}$·$(\mathbf{1_C})_2$), H''_b ([4 + 2]-*anti*-$\mathbf{2_{CC}}$), H''_b ([4 + 4]-*anti*-$\mathbf{2_{CC}}$) and the internal standard (1,1,2,2-tetrachloroethane) based on

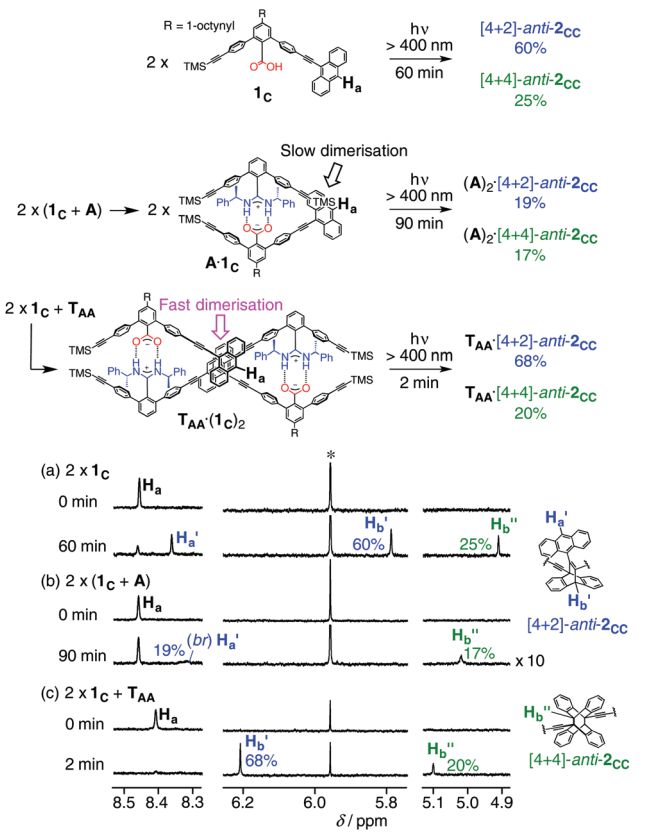

Fig. 6 Partial ^{1}H NMR (500 MHz, degassed $CDCl_3$, 25 °C) spectra of $\mathbf{1_C}$ (0.50 mM) in the absence (run 4 in Table 2) (a) and presence of **A** (0.50 mM) (run 5 in Table 2) (b) and $\mathbf{T_{AA}}$ (0.25 mM) (run 6 in Table 2) (c) before (top) and after (bottom) irradiation of light (>400 nm). * denotes the peak due to 1,1,2,2-tetrachloroethane used as an internal standard. Full-scale spectra are shown in Fig. S21a, S22a and S25a.† The peaks for $(\mathbf{A})_2$·[4 + 2]-*anti*-$\mathbf{2_{CC}}$ were too broad to estimate its yield. The yield of $(\mathbf{A})_2$·[4 + 2]-*anti*-$\mathbf{2_{CC}}$ was estimated to be 19% from the integral ratios of the peaks for isolated [4 + 4]-*anti*-$\mathbf{2_{CC}}$ and [4 + 2]-*anti*-$\mathbf{2_{CC}}$ (see Fig. S22b†).

the ^{1}H NMR spectral changes and were plotted *versus* the reaction time (Fig. 7, S21, S23 and S25†). The experimental data were then fitted to a first-order kinetic model using eqn (1),

$$\ln(C/C_0) = -kt \quad (1)$$

where C is the concentration of $\mathbf{1_C}$, and t is the reaction time. As shown in Fig. 7, the photodimerisation was significantly accelerated in the presence of $\mathbf{T_{AA}}$ probably because of the close proximity of the anthracene moiety of $\mathbf{1_C}$ along the template (Fig. S26†). The k values in the presence and absence of $\mathbf{T_{AA}}$ were then estimated to be 20×10^{-3} s^{-1} and 0.66×10^{-3} s^{-1}, respectively, by the least-squares curve fitting method as shown in Fig. 7. Thus, the photodimerisation of $\mathbf{1_C}$ was remarkably accelerated 30-fold ($k(\mathbf{T_{AA}}\cdot(\mathbf{1_C})_2)/k(\mathbf{1_C}) = 30$) in the presence of $\mathbf{T_{AA}}$ through the salt bridges, although the template-directed regioselectivity control during the photoreaction was not achieved.

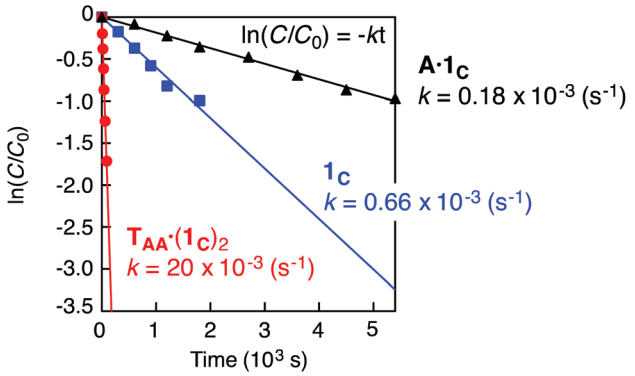

Fig. 7 Kinetic plots of the photodimerisation of $\mathbf{1_C}$ (0.50 mM) in degassed $CDCl_3$ at 25 °C in the absence (blue line) and presence of **A** (black line) and $\mathbf{T_{AA}}$ (red line). The reaction rates were estimated from the integral ratios of the peaks for H_a ($\mathbf{1_C}$) and the internal standard (1,1,2,2-tetrachloroethane) based on the ^{1}H NMR spectral changes shown in Fig. S21a, S22a and S25a.†

In the presence of **A**, however, the photodimerisation (run 5 in Table 2) of $\mathbf{1_C}$ took place very slowly with the k value of 0.18×10^{-3} s^{-1} (Fig. 7 and S23†). The ^{1}H NMR spectrum of $\mathbf{A}\cdot\mathbf{1_C}$ after irradiation for 90 min was rather complicated except for the signals of $(\mathbf{A})_2\cdot$[4 + 4]-*anti*-$\mathbf{2_{CC}}$ (17%), and those of $(\mathbf{A})_2\cdot$[4 + 2]-*anti*-$\mathbf{2_{CC}}$ were not clearly observed because the signals were too broad (Fig. 6b and S22a†). The resulting photodimers with carboxylic acid residues were then isolated from the reaction mixture by silica gel column chromatography and the yield of $(\mathbf{A})_2\cdot$[4 + 2]-*anti*-$\mathbf{2_{CC}}$ was estimated to be 19% based on the integral ratio ([4 + 2]-*anti*-$\mathbf{2_{CC}}$/[4 + 4]-*anti*-$\mathbf{2_{CC}}$) in the ^{1}H NMR spectrum (Fig. S22b†). Molecular mechanics (MM) calculations for the $\mathbf{A}\cdot\mathbf{1_C}$ salt-bridged complex suggested that one of the terminal TMS units of **A** is located close to the anthracene moiety of $\mathbf{1_C}$ and a reactive acetylene residue of $\mathbf{1_C}$ is likely sandwiched between the TMS and the phenyl group of the amidine residue of **A** (Fig. S24†). Thus, the photodimerisation of $\mathbf{1_C}$, in particular, the formation of [4 + 2]-*anti*-$\mathbf{2_{CC}}$ may be considerably retarded once complexed with **A** due to such steric effects, leading to the decrease in the reaction rate.

Template effects on the photoreactions of di-9-phenylethynylanthracene-bound carboxylic acid monomer

The photoreactions of the di-9-phenylethynylanthracene-bound carboxylic acid monomer ($\mathbf{3_C}$) (0.50 mM) in the absence and presence of the template $\mathbf{T_{AA}}$ (0.25 mM) were also investigated in undegassed and degassed $CDCl_3$ at 25 °C (Table 3). The irradiation of $\mathbf{3_C}$ in undegassed $CDCl_3$ (run 1 in Table 3 and Fig. S29†) readily promoted the photooxidation to produce a mixture of mono- ($\mathbf{3_C}$-O_2) and di-endoperoxides ($\mathbf{3_C}$-$2O_2$) in 50% yield as identified by the ESI-mass (Fig. S29c†) and NMR analysis (Fig. S1†), which eventually reverted to the parent $\mathbf{3_C}$ and further converted in part to unknown compounds by

Table 3 Results of photoreactions of **3C**

	$\mathbf{3_C}$				Products yield (%) (reaction rate 10^{-3} k (s^{-1}))						
					poly-$\mathbf{3_C}$						
Run	Additive (conc. (mM))	Solvent (conc. (mM))	Irradiation time (min)	Conv. (%) (consumption rate 10^{-3} k (s^{-1}))	[4 + 2]-*anti*	[4 + 4]-*anti*	$\mathbf{3_C}$-O_2 and $\mathbf{3_C}$-$2O_2$	[4 + 2]-*anti*-$\mathbf{4_{CC}}$	[4 + 4]-*anti*-$\mathbf{4_{CC}}$	[4 + 2]/[4 + 4]	Sup. Fig. no.
1	—	Undegassed $CDCl_3$ (0.50)	3	82 (9.9)	—		50[a] (4.2)	—	—	—	Fig. S29
2	$\mathbf{T_{AA}}$ (0.25)	Undegassed $CDCl_3$ (0.50)	2	97 (38)	—		12 (1.4)	60[b] (19)	17[b] (3.6)	3.5	Fig. S31–34
3	—	Degassed $CDCl_3$ (0.50)	60	22[c] (0.61)[c]	72[d] $M_n = 3.2 \times 10^3$		—	—[e]	—[e]	3.0	Fig. S35
					54 (0.39)	18 (0.010)					
4	$\mathbf{T_{AA}}$ (0.25)	Degassed $CDCl_3$ (0.50)	2	95 (37)	—		—	74 (23)	20 (4)	3.7	Fig. S36–38

[a] Total yield of mono- ($\mathbf{3C}$-O_2) and di-endoperoxides ($\mathbf{3C}$-$2O_2$) of **3C**, which were gradually converted into unknown compounds probably due to photolysis upon further photoirradiation (see Fig. S30). [b] One of the terminal anthracene units of [4 + 2]- and [4 + 4]-*anti*-**4CC** was oxidised (see Fig. S31). [c] The conversion of **3C** and its consumption rate were estimated based on the formation of poly-**3C** using ^{1}H NMR (see Fig. S35a). [d] The number-average molecular weight (M_n) was determined by SEC using polystyrene standards in THF containing 0.1 wt% TBAB as the eluent (see Fig. 8B(a)). [e] It was difficult to estimate the yields of [4 + 2]- and [4 + 4]-*anti*-**4CC** because their proton NMR signals were overlapped with those of poly-**3C** (see Fig. S35a).

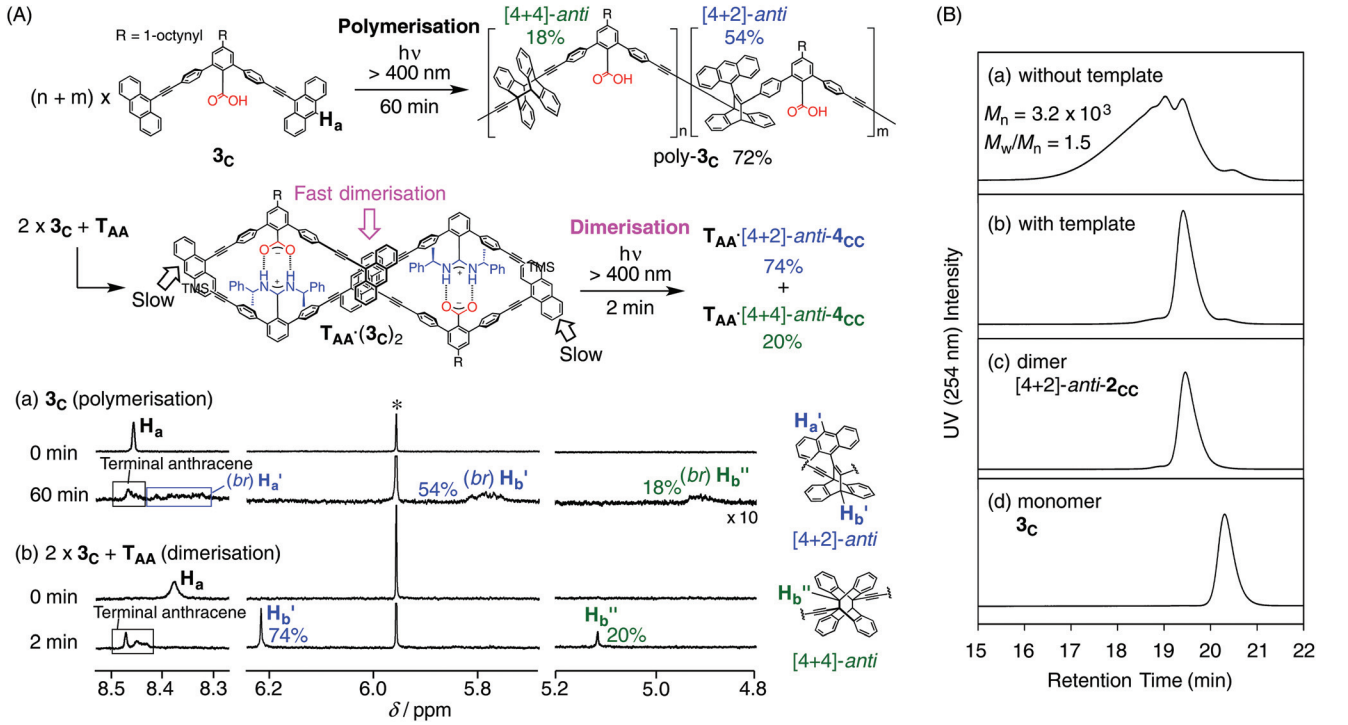

Fig. 8 (A) Partial ^{1}H NMR (500 MHz, degassed $CDCl_3$, 25 °C) spectra of $\mathbf{3_C}$ (0.50 mM) in the absence (run 3 in Table 3) (a) and presence of $\mathbf{T_{AA}}$ (run 4 in Table 3) (b) before (top) and after (bottom) irradiation of light (>400 nm). * denotes the peak due to 1,1,2,2-tetrachloroethane used as an internal standard. Full-scale spectra are shown in Fig. S35a and S36a.† (B) SEC chromatograms of (a) poly-$\mathbf{3_C}$ produced in a degassed $CDCl_3$ solution of $\mathbf{3_C}$ (0.50 mM) upon irradiation with light (>400 nm) for 60 min (see Fig. S35†), (b) isolated carboxylic acid dimers obtained from $\mathbf{T_{AA}}\cdot(\mathbf{3_C})_2$ (0.25 mM) after irradiation of light (>400 nm) for 120 s in degassed $CDCl_3$ (see Fig. S37g†), (c) dimer [4 + 2]-*anti*-$\mathbf{2_{CC}}$, and (d) monomer $\mathbf{3_C}$. These carboxylic acids were converted into the corresponding methyl esters by treatment with (trimethylsilyl)diazomethane before SEC analysis.

thermolysis (Fig. S30†). In the presence of $\mathbf{T_{AA}}$, the photooxidation of $\mathbf{3_C}$ was significantly suppressed as anticipated (12% yield, run 2 in Table 3)[22] and the [4 + 2]- and [4 + 4]-*anti*-$\mathbf{4_{CC}}$ photodimers were mainly produced in 60 and 17% yields, respectively, on the basis of the ^{1}H NMR spectra of the products by comparing them with those of the photodimers of $\mathbf{2_{CC}}$ formed in the presence of $\mathbf{T_{AA}}$ (Fig. S37a–d†). We found that one of the terminal anthracene units of $\mathbf{4_{CC}}$ complexed with $\mathbf{T_{AA}}$ was further oxidised (Fig. S31b†), resulting in the formation of the mono- and/or dioxidised dimers, [4 + 2]-*anti*-$\mathbf{4_{CC}}$-O_2 and [4 + 4]-*anti*-$\mathbf{4_{CC}}$-O_2.

In strong contrast, the ^{1}H NMR spectrum of $\mathbf{3_C}$ (0.50 mM) after irradiation for 60 min in degassed $CDCl_3$ (run 3 in Table 3) became significantly broadened, giving signals due to the [4 + 2]- and [4 + 4]-*anti* dimerisations (H′$_b$ and H″$_b$), indicating the formation of a random copolymer (poly-$\mathbf{3_C}$) composed of [4 + 2]- and [4 + 4]-*anti* units (Fig. 8A(a) and S35a†). The size-exclusion chromatography (SEC) analysis further supported the polymerisation of $\mathbf{3_C}$ (Fig. 8B(a)).[23] Interestingly, the photoreaction of $\mathbf{T_{AA}}\cdot(\mathbf{3_C})_2$ in degassed $CDCl_3$ (run 4 in Table 3) showed two sharp bridge-head peaks (H′$_b$ and H″$_b$), suggesting the formation of the photodimers, $\mathbf{T_{AA}}\cdot$[4 + 2]-*anti*-$\mathbf{4_{CC}}$ and $\mathbf{T_{AA}}\cdot$[4 + 4]-*anti*-$\mathbf{4_{CC}}$, while the other anthracene moieties remained unreacted as evidenced by the ^{1}H NMR and absorption spectra (Fig. 8A(b), S36a and S38†). The SEC analysis of the products further supported this conclusion (Fig. 8B(b–d)).

These results indicated that the dimeric template $\mathbf{T_{AA}}$ selectively promoted the photodimerisation of the anthracene units of the bimolecular $\mathbf{3_C}$ located in close proximity at the center (Fig. S38†), whereas the further polymerisation of the resultant $\mathbf{T_{AA}}\cdot$[4 + 2]-*anti*-$\mathbf{4_{CC}}$ and $\mathbf{T_{AA}}\cdot$[4 + 4]-*anti*-$\mathbf{4_{CC}}$ dimers was exclusively protected due to the steric effects between the remaining anthracene units at the ends and the TMS and phenyl groups of the amidine residues of $\mathbf{T_{AA}}$ as observed in the photodimerisation of $\mathbf{A}\cdot\mathbf{1_C}$ (run 5 in Table 2).

In the same way, the k values of $\mathbf{3_C}$ in degassed $CDCl_3$ in the presence and absence of $\mathbf{T_{AA}}$ were estimated to be 37×10^{-3} s^{-1} and 0.61×10^{-3} s^{-1}, respectively, (Fig. S35d and S36c†). Thus, the photodimerisation of $\mathbf{3_C}$ was accelerated 61-fold ($k(\mathbf{T_{AA}}\cdot(\mathbf{3_C})_2)/k(\mathbf{3_C}) = 61$) in the presence of $\mathbf{T_{AA}}$. Moreover, the dimerisation of $\mathbf{3_C}$ was found to take place faster than that of $\mathbf{1_C}$ in the presence of $\mathbf{T_{AA}}$ by a factor of 1.9 ($k(\mathbf{T_{AA}}\cdot(\mathbf{3_C})_2)/k(\mathbf{T_{AA}}\cdot(\mathbf{1_C})_2) = 1.9$). This indicated that $\mathbf{3_C}$ can more effectively dimerise along the template than $\mathbf{1_C}$ because $\mathbf{3_C}$ possesses two anthracene moieties at both ends (Fig. S37e†).

Conclusions

In conclusion, we have performed a close inspection of the photochemical reactions of 9-phenylethynylanthracene under

various reaction conditions and proved the [4 + 4]-*anti* and [4 + 2]-*anti* dimers structures produced during the photodimerisation[13] by single-crystal X-ray analysis. We also found a remarkable template effect of the amidine dimer on the photoreactions of the mono- and di-9-phenylethynylanthracene-bound carboxylic acid monomers. The detailed kinetic and structural studies revealed that the [4 + 4]- and [4 + 2]-*anti* photodimers ($\mathbf{2}_{CC}$ and $\mathbf{4}_{CC}$) were selectively produced along the template and the reaction rate was accelerated 30 or 61-fold without side reactions, oxidation and polymerisation. The observed noticeable enhancement of the dimerisation rate constants could be ascribed to the two anthracene moieties of the monomers located in close proximity at the reaction site along the rigid template assisted by the amidinium–carboxylate salt bridges. Although the template-directed, specific regioselective-photodimerisation was not achieved, the present template-directed photodimerisation system based on salt bridges will be further applied to the template-directed enantioselective photodimerisation of prochiral anthracene derivatives[10,24] because the amidine dimer used in the present study is optically active.[25] Studies along this line are now underway in our laboratory.

Acknowledgements

This work was supported in part by JSPS KAKENHI (Grant-in-Aid for Scientific Research (S), No. 25220804 (E. Y.) and Grant-in-Aid for Young Scientists (B), No. 26810048 (D. T.)). J. T. expresses his thanks for the JSPS Research Fellowship for Young Scientists (No. 8886). The authors thank Professor Hiroki Iida for his help with the single crystal X-ray diffraction analysis.

Notes and references

1 (*a*) N. Hoffmann, *Chem. Rev.*, 2008, **108**, 1052–1103; (*b*) T. Bach and J. P. Hehn, *Angew. Chem., Int. Ed.*, 2011, **50**, 1000–1045; (*c*) N. Hoffmann, *J. Photochem. Photobiol., C*, 2014, **19**, 1–19; (*d*) N. Hoffmann, *Synthesis*, 2016, 1782–1802.

2 (*a*) N. D. McClenaghan and D. M. Bassani, *Int. J. Photoenergy*, 2004, **6**, 185–192; (*b*) J. Svoboda and B. König, *Chem. Rev.*, 2006, **106**, 5413–5430; (*c*) C. Yang, *Chin. Chem. Lett.*, 2013, **24**, 437–441; (*d*) B. Bibal, C. Mongin and D. M. Bassani, *Chem. Soc. Rev.*, 2014, **43**, 4179–4198; (*e*) N. Vallavoju and J. Sivaguru, *Chem. Soc. Rev.*, 2014, **43**, 4084–4101; (*f*) C. Yang and Y. Inoue, *Chem. Soc. Rev.*, 2014, **43**, 4123–4143; (*g*) R. Brimioulle, D. Lenhart, M. M. Maturi and T. Bach, *Angew. Chem., Int. Ed.*, 2015, **54**, 3872–3890; (*h*) V. Ramamurthy and J. Sivaguru, *Chem. Rev.*, 2016, **116**, 9914–9993.

3 (*a*) H.-D. Becker, *Chem. Rev.*, 1993, **93**, 145–172; (*b*) H. Bouas-Laurent, A. Castellan, J.-P. Desvergne and R. Lapouyade, *Chem. Soc. Rev.*, 2000, **29**, 43–55; (*c*) H. Bouas-Laurent, A. Castellan, J.-P. Desvergne and R. Lapouyade, *Chem. Soc. Rev.*, 2001, **30**, 248–263.

4 (*a*) P. Kissel, R. Erni, W. B. Schweizer, M. D. Rossell, B. T. King, T. Bauer, S. Götzinger, A. D. Schlüter and J. Sakamoto, *Nat. Chem.*, 2012, **4**, 287–291; (*b*) R. Bhola, P. Payamyar, D. J. Murray, B. Kumar, A. J. Teator, M. U. Schmidt, S. M. Hammer, A. Saha, J. Sakamoto, A. D. Schlüter and B. T. King, *J. Am. Chem. Soc.*, 2013, **135**, 14134–14141; (*c*) P. Kissel, D. J. Murray, W. J. Wulftange, V. J. Catalano and B. T. King, *Nat. Chem.*, 2014, **6**, 774–778; (*d*) M. J. Kory, M. Wörle, T. Weber, P. Payamyar, S. W. van de Poll, J. Dshemuchadse, N. Trapp and A. D. Schlüter, *Nat. Chem.*, 2014, **6**, 779–784; (*e*) P. Payamyar, K. Kaja, C. Ruiz-Vargas, A. Stemmer, D. J. Murray, C. J. Johnson, B. T. King, F. Schiffmann, J. VandeVondele, A. Renn, S. Götzinger, P. Ceroni, A. Schütz, L.-T. Lee, Z. Zheng, J. Sakamoto and A. D. Schlüter, *Adv. Mater.*, 2014, **26**, 2052–2058; (*f*) D. J. Murray, D. D. Patterson, P. Payamyar, R. Bhola, W. Song, M. Lackinger, A. D. Schlüter and B. T. King, *J. Am. Chem. Soc.*, 2015, **137**, 3450–3453; (*g*) P. Payamyar, M. Servalli, T. Hungerland, A. P. Schütz, Z. Zheng, A. Borgschulte and A. D. Schlüter, *Macromol. Rapid Commun.*, 2015, **36**, 151–158.

5 (*a*) J.-F. Xu, Y.-Z. Chen, L.-Z. Wu, C.-H. Tung and Q.-Z. Yang, *Org. Lett.*, 2013, **15**, 6148–6151; (*b*) P. Wang, J. Hu, S. Yang, B. Song and Q. Wang, *Chem. – Asian J.*, 2014, **9**, 2880–2884; (*c*) P. Wei, X. Yan and F. Huang, *Chem. Commun.*, 2014, **50**, 14105–14108; (*d*) Z. Ji, Y. Li, Y. Ding, G. Chen and M. Jiang, *Polym. Chem.*, 2015, **6**, 6880–6884; (*e*) Z. Yu, J. Zhang, R. J. Coulston, R. M. Parker, F. Biedermann, X. Liu, O. A. Scherman and C. Abell, *Chem. Sci.*, 2015, **6**, 4929–4933; (*f*) X. Zhang, Y. Gao, Y. Lin, J. Hu and Y. Ju, *Polym. Chem.*, 2015, **6**, 4162–4166.

6 (*a*) Y. Zheng, M. Micic, S. V. Mello, M. Mabrouki, F. M. Andreopoulos, V. Konka, S. M. Pham and R. M. Leblanc, *Macromolecules*, 2002, **35**, 5228–5234; (*b*) L. A. Connal, R. Vestberg, C. J. Hawker and G. G. Qiao, *Adv. Funct. Mater.*, 2008, **18**, 3315–3322; (*c*) P. Froimowicz, H. Frey and K. Landfester, *Macromol. Rapid Commun.*, 2011, **32**, 468–473; (*d*) L. A. Wells, M. A. Brook and H. Sheardown, *Macromol. Biosci.*, 2011, **11**, 988–998; (*e*) F. Biedermann, I. Ross and O. A. Scherman, *Polym. Chem.*, 2014, **5**, 5375–5382; (*f*) L. López-Vilanova, I. Martinez, T. Corrales and F. Catalina, *Eur. Polym. J.*, 2014, **56**, 69–76; (*g*) H. Xie, C.-Y. Cheng, L. Du, C.-J. Fan, X.-Y. Deng, K.-K. Yang and Y.-Z. Wang, *Macromolecules*, 2016, **49**, 3845–3855; (*h*) H. Xie, M.-J. He, X.-Y. Deng, L. Du, C.-J. Fan, K.-K. Yang and Y.-Z. Wang, *ACS Appl. Mater. Interfaces*, 2016, **8**, 9431–9439.

7 (*a*) F. Moriwaki, A. Ueno, T. Osa, F. Hamada and K. Murai, *Chem. Lett.*, 1986, 1865–1868; (*b*) Y. Molard, D. M. Bassani, J.-P. Desvergne, P. N. Horton, M. B. Hursthouse and J. H. R. Tucker, *Angew. Chem., Int. Ed.*, 2005, **44**, 1072–1075; (*c*) C. Schäfer, R. Eckel, R. Ros, J. Mattay and D. Anselmetti, *J. Am. Chem. Soc.*, 2007, **129**, 1488–1489; (*d*) C.-K. Liang, G. V. Dubacheva, T. Buffeteau, D. Cavagnat, P. Hapiot,

B. Fabre, J. H. R. Tucker and D. M. Bassani, *Chem. – Eur. J.*, 2013, **19**, 12748–12758; (*e*) H. Wang, F. Liu, R. C. Helgeson and K. N. Houk, *Angew. Chem., Int. Ed.*, 2013, **52**, 655–659.

8 (*a*) R. O. Al-Kaysi, A. M. Müller and C. J. Bardeen, *J. Am. Chem. Soc.*, 2006, **128**, 15938–15939; (*b*) R. O. Al-Kaysi and C. J. Bardeen, *Adv. Mater.*, 2007, **19**, 1276–1280; (*c*) J. T. Good, J. J. Burdett and C. J. Bardeen, *Small*, 2009, **5**, 2902–2909; (*d*) L. Zhu, R. O. Al-Kaysi and C. J. Bardeen, *J. Am. Chem. Soc.*, 2011, **133**, 12569–12575; (*e*) T. Kim, L. Zhu, L. J. Mueller and C. J. Bardeen, *J. Am. Chem. Soc.*, 2014, **136**, 6617–6625.

9 (*a*) T. Wolff, *J. Photochem.*, 1981, **16**, 343–346; (*b*) T. Wolff and N. Müller, *J. Photochem.*, 1983, **23**, 131–140; (*c*) T. Wolff, N. Müller and G. von Bünau, *J. Photochem.*, 1983, **22**, 61–70; (*d*) A. Schütz and T. Wolff, *J. Photochem. Photobiol., A*, 1997, **109**, 251–258.

10 (*a*) T. Tamaki, *Chem. Lett.*, 1984, **13**, 53–56; (*b*) T. Tamaki and T. Kokubu, *J. Inclusion Phenom.*, 1984, **2**, 815–822; (*c*) A. Ueno, F. Moriwaki, Y. Iwama, I. Suzuki, T. Osa, T. Ohta and S. Nozoe, *J. Am. Chem. Soc.*, 1991, **113**, 7034–7036; (*d*) A. Nakamura and Y. Inoue, *J. Am. Chem. Soc.*, 2003, **125**, 966–972; (*e*) C. Yang, A. Nakamura, G. Fukuhara, Y. Origane, T. Mori, T. Wada and Y. Inoue, *J. Org. Chem.*, 2006, **71**, 3126–3136; (*f*) C. Yang, T. Mori, Y. Origane, Y. H. Ko, N. Selvapalam, K. Kim and Y. Inoue, *J. Am. Chem. Soc.*, 2008, **130**, 8574–8575; (*g*) C. Ke, C. Yang, T. Mori, T. Wada, Y. Liu and Y. Inoue, *Angew. Chem., Int. Ed.*, 2009, **48**, 6675–6677; (*h*) C. Yang, C. Ke, W. Liang, G. Fukuhara, T. Mori, Y. Liu and Y. Inoue, *J. Am. Chem. Soc.*, 2011, **133**, 13786–13789; (*i*) J. Yao, Z. Yan, J. Ji, W. Wu, C. Yang, M. Nishijima, G. Fukuhara, T. Mori and Y. Inoue, *J. Am. Chem. Soc.*, 2014, **136**, 6916–6919.

11 T. Ihara, T. Fujii, M. Mukae, Y. Kitamura and A. Jyo, *J. Am. Chem. Soc.*, 2004, **126**, 8880–8881.

12 (*a*) N. Sugiyama, M. Iwata, M. Yoshioka, K. Yamada and H. Aoyama, *Bull. Chem. Soc. Jpn.*, 1969, **42**, 1377–1379; (*b*) N. J. Turro, M.-F. Chow and J. Rigaudy, *J. Am. Chem. Soc.*, 1981, **103**, 7218–7224; (*c*) N. Toshima, T. Sugano and H. Hirai, *Can. J. Chem.*, 1984, **62**, 2047–2053; (*d*) J.-M. Aubry, C. Pierlot, J. Rigaudy and R. Schmidt, *Acc. Chem. Res.*, 2003, **36**, 668–675; (*e*) E. Berni, C. Dolain, B. Kauffmann, J.-M. Léger, C. Zhan and I. Huc, *J. Org. Chem.*, 2008, **73**, 2687–2694; (*f*) W. Fudickar and T. Linker, *J. Am. Chem. Soc.*, 2012, **134**, 15071–15082.

13 H.-D. Becker and K. Andersson, *J. Photochem.*, 1984, **26**, 75–77.

14 (*a*) M. Kim, J. N. Hohman, Y. Cao, K. N. Houk, H. Ma, A. K.-Y. Jen and P. S. Weiss, *Science*, 2011, **331**, 1312–1315; (*b*) Y. B. Zheng, J. L. Payton, T.-B. Song, B. K. Pathem, Y. Zhao, H. Ma, Y. Yang, L. Jensen, A. K.-Y. Jen and P. S. Weiss, *Nano Lett.*, 2012, **12**, 5362–5368.

15 T. Zdobinsky, P. S. Maiti and R. Klajn, *J. Am. Chem. Soc.*, 2014, **136**, 2711–2714.

16 (*a*) Y. Tanaka, H. Katagiri, Y. Furusho and E. Yashima, *Angew. Chem., Int. Ed.*, 2005, **44**, 3867–3870; (*b*) Y. Furusho, Y. Tanaka and E. Yashima, *Org. Lett.*, 2006, **8**, 2583–2586; (*c*) M. Ikeda, Y. Tanaka, T. Hasegawa, Y. Furusho and E. Yashima, *J. Am. Chem. Soc.*, 2006, **128**, 6806–6807; (*d*) Y. Furusho, Y. Tanaka, T. Maeda, M. Ikeda and E. Yashima, *Chem. Commun.*, 2007, 3174–3176; (*e*) T. Hasegawa, Y. Furusho, H. Katagiri and E. Yashima, *Angew. Chem., Int. Ed.*, 2007, **46**, 5885–5888; (*f*) H. Ito, Y. Furusho, T. Hasegawa and E. Yashima, *J. Am. Chem. Soc.*, 2008, **130**, 14008–14015; (*g*) T. Maeda, Y. Furusho, S.-i. Sakurai, J. Kumaki, K. Okoshi and E. Yashima, *J. Am. Chem. Soc.*, 2008, **130**, 7938–7945; (*h*) H. Iida, M. Shimoyama, Y. Furusho and E. Yashima, *J. Org. Chem.*, 2010, **75**, 417–423; (*i*) H. Yamada, Y. Furusho, H. Ito and E. Yashima, *Chem. Commun.*, 2010, **46**, 3487–3489; (*j*) H. Ito, M. Ikeda, T. Hasegawa, Y. Furusho and E. Yashima, *J. Am. Chem. Soc.*, 2011, **133**, 3419–3432; (*k*) H. Yamada, Y. Furusho and E. Yashima, *J. Am. Chem. Soc.*, 2012, **134**, 7250–7253; (*l*) H. Yamada, Z.-Q. Wu, Y. Furusho and E. Yashima, *J. Am. Chem. Soc.*, 2012, **134**, 9506–9520; (*m*) J. Tanabe, D. Taura, H. Yamada, Y. Furusho and E. Yashima, *Chem. Sci.*, 2013, **4**, 2960–2966; (*n*) M. Horie, N. Ousaka, D. Taura and E. Yashima, *Chem. Sci.*, 2015, **6**, 714–723.

17 C.-W. Wan, A. Burghart, J. Chen, F. Bergstrom, L. B.-Å. Johansson, M. F. Wolford, T. G. Kim, M. R. Topp, R. M. Hochstrasser and K. Burgess, *Chem. – Eur. J.*, 2003, **9**, 4430–4441.

18 (*a*) Y. Shiraishi, S. Kanazawa, Y. Sugano, D. Tsukamoto, H. Sakamoto, S. Ichikawa and T. Hirai, *ACS Catal.*, 2014, **4**, 774–780; (*b*) H. Zhang, L.-H. Guo, L. Zhao, B. Wan and Y. Yang, *J. Phys. Chem. Lett.*, 2015, **6**, 958–963.

19 The photooxidised $\mathbf{1_C}$-O_2 gradually decomposed under shielded light, producing the monomer $\mathbf{1_C}$ together with a small amount of an unknown compound (Fig. S17†).

20 The association constant (K_a) between $\mathbf{1_C}$ and **A** could be roughly estimated to be *ca.* 3.5×10^6 M^{-1} in $CDCl_3$ by comparison of the K_a value between analogous amidine and carboxylic acids.[16]

21 The template $\mathbf{T_{AA}}$ possesses four alkyne units that are not bonded to the anthracene residue. However, these alkyne units did not participate in the photoreactions because the conversion (89%) of $\mathbf{1_C}$ after photoirradiation for 2 min in the presence of $\mathbf{T_{AA}}$ is almost consistent with the total yield (68 and 20%) of the resulting carboxylic acid photodimers ([4 + 2]-*anti*-$\mathbf{2_{CC}}$ and [4 + 4]-*anti*-$\mathbf{2_{CC}}$) (run 6 in Table 2). In addition, the structures of the dimer products isolated were fully characterised, indicating that the photodimers were not composed of $\mathbf{T_{AA}}$ at all. Becker and Andersson also reported that the intermolecular photodimerisation between anthracene and diphenylacetylene did not take place, giving no [4 + 2]-cycloadduct upon light irradiation over 400 nm.[13] This also suggests that the alkyne units of $\mathbf{T_{AA}}$ will not react with the anthracene unit(s) of $\mathbf{1_C}$ and $\mathbf{3_C}$ upon photoirradiation (>400 nm).

22 The peak assignments were performed by comparing the ^{1}H NMR spectrum of a mixture of $\mathbf{3_C}$-O_2 and $\mathbf{3_C}$-$2O_2$ in the presence of $\mathbf{T_{AA}}$ (Fig. S33†).

23 Poly-$\mathbf{3_C}$ was converted to the corresponding methyl esters by treatment with (trimethylsilyl)diazomethane. The number average molecular weight (M_n) and its distribution (M_w/M_n) were estimated to be 3.2×10^3 and 1.5, respectively, by SEC using polystyrene standards and THF containing 0.1 wt% tetrabutylammonium bromide as the eluent. The M_n value corresponds to *ca.* 4 repeating units in a single polymer chain.

24 (*a*) Y. Ishida, Y. Kai, S.-y. Kato, A. Misawa, S. Amano, Y. Matsuoka and K. Saigo, *Angew. Chem., Int. Ed.*, 2008, **47**, 8241–8245; (*b*) A. Dawn, T. Shiraki, S. Haraguchi, H. Sato, K. Sada and S. Shinkai, *Chem. – Eur. J.*, 2010, **16**, 3676–3689; (*c*) Y. Ishida, A. S. Achalkumar, S.-y. Kato, Y. Kai, A. Misawa, Y. Hayashi, K. Yamada, Y. Matsuoka, M. Shiro and K. Saigo, *J. Am. Chem. Soc.*, 2010, **132**, 17435–17446; (*d*) D. Fuentealba, H. Kato, M. Nishijima, G. Fukuhara, T. Mori, Y. Inoue and C. Bohne, *J. Am. Chem. Soc.*, 2013, **135**, 203–209; (*e*) Y. Ishida, Y. Matsuoka, Y. Kai, K. Yamada, K. Nakagawa, T. Asahi and K. Saigo, *J. Am. Chem. Soc.*, 2013, **135**, 6407–6410; (*f*) Y. Kawanami, H. Umehara, J.-i. Mizoguchi, M. Nishijima, G. Fukuhara, C. Yang, T. Mori and Y. Inoue, *J. Org. Chem.*, 2013, **78**, 3073–3085; (*g*) G. Fukuhara, H. Umehara, S. Higashino, M. Nishijima, C. Yang, T. Mori, T. Wada and Y. Inoue, *Photochem. Photobiol. Sci.*, 2014, **13**, 162–171; (*h*) G. Fukuhara, K. Iida, Y. Kawanami, H. Tanaka, T. Mori and Y. Inoue, *J. Am. Chem. Soc.*, 2015, **137**, 15007–15014; (*i*) G. Fukuhara, K. Iida, T. Mori and Y. Inoue, *J. Photochem. Photobiol., A*, 2016, **331**, 76–83; (*j*) M. M. Maturi, G. Fukuhara, K. Tanaka, Y. Kawanami, T. Mori, Y. Inoue and T. Bach, *Chem. Commun.*, 2016, **52**, 1032–1035.

25 The complexes of the achiral $\mathbf{1_C}$ and $\mathbf{3_C}$ with the optically active amidine template $\mathbf{T_{AA}}$ exhibited apparent Cotton effects in the absorption region of the anthracene residues (*ca.*, 350–440 nm) accompanied by a decrease and red-shift in their absorption spectra (Fig. S20, S26, S34 and S38†), indicating that the two anthracene units of the monomers appear to be arranged in a chiral fashion along the chiral template. These results seem to be promising for realising such a template-directed enantioselective photodimerisation.